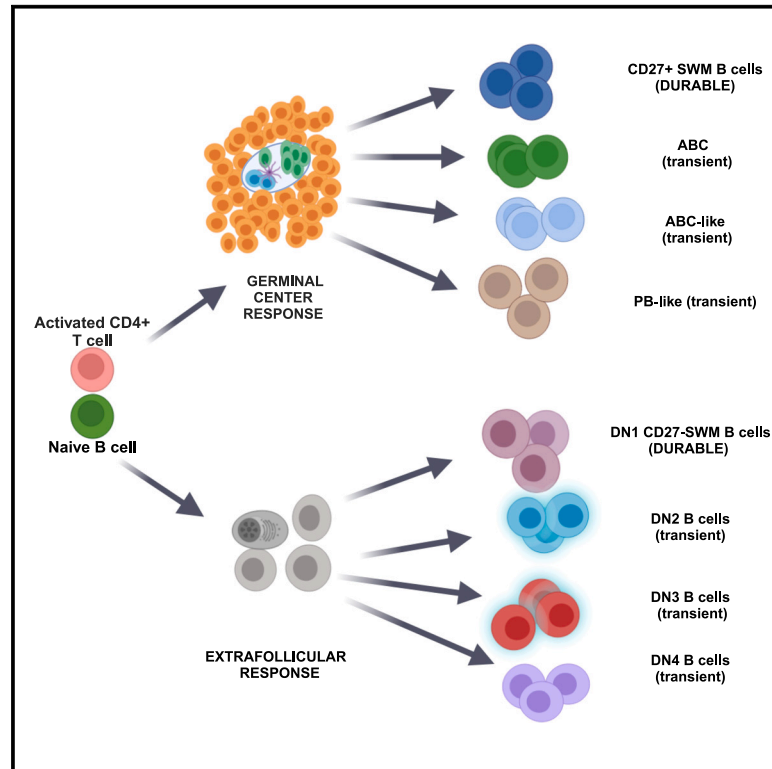**Article**

Two distinct durable human class-switched memory B cell populations are induced by vaccination and infection

Graphical abstract

Authors

Cory A. Perugino, Hang Liu,
Jared Feldman, ..., Vivek Naranbhai,
Aaaron G. Schmidt, Shiv Pillai

Correspondence

spillai@mgh.harvard.edu

In brief

Perugino et al. examined the durability of all class-switched human B cells after vaccination and identified IgD⁻CXCR5⁺CD11c⁻CD27⁻ DN1 B cells as durable B cells, less somatically mutated and more clonally expanded than germinal center-derived IgD⁻CXCR5⁺CD11c⁻CD27⁺ memory B cells. These extrafollicular B cells exhibit a TP63 linked transcriptional signature.

Highlights

- Most class-switched B cell subsets including ABCs, DN2, and DN3 B cells are non-durable

- IgD⁻CXCR5⁺CD11c⁻CD27⁻ DN1 B cells are a non-germinal center-derived durable B cell subset

- DN1 B cells have lower SHM but are more clonally expanded than CD27⁺ durable memory B cells

- DN1 B cells exhibit a TP63 transcriptional signature

CellPress

Two distinct durable human class-switched memory B cell populations are induced by vaccination and infection

Cory A. Perugino,[1,2] Hang Liu,[1] Jared Feldman,[1] Jess Marbourg,[3] Thomas V. Guy,[1] Anson Hui,[1] Nicole Ingram,[1] Julian Liebaert,[1] Neha Chaudhary,[3] Weiyang Tao,[3] Catherine Jacob-Dolan,[1,11] Blake M. Hauser,[1] Zayd Mian,[1] Anusha Nathan,[1] Zezhou Zhao,[1] Clarety Kaseke,[1] Rhoda Tano-Menka,[1] Matthew A. Getz,[1] Fernando Senjobe,[1] Cristhian Berrios,[4] Onosereme Ofoman,[4] Zachary Manickas-Hill,[1] Duane R. Wesemann,[5] Jacob E. Lemieux,[6,7] Marcia B. Goldberg,[6,7,13] Kerstin Nündel,[8] Ann Moormann,[8] Ann Marshak-Rothstein,[8] Regina C. Larocque,[6] Edward T. Ryan,[6] John A. Iafrate,[10] Daniel Lingwood,[1] Gaurav Gaiha,[1,9] Richelle Charles,[6] Alejandro B. Balazs,[1] Aridaman Pandit,[3] Vivek Naranbhai,[10,11,12] Aaaron G. Schmidt,[1,13] and Shiv Pillai[1,14,*]

[1]Ragon Institute of MGH, MIT and Harvard, Cambridge, MA 02139, USA
[2]Division of Rheumatology Allergy and Immunology, Massachusetts General Hospital, Boston, MA 02114, USA
[3]Abbvie Cambridge Research Center, Cambridge, MA 02139, USA
[4]Department of Pathology, Massachusetts Hospital, Boston, MA 02114, USA
[5]Department of Medicine, Brigham and Women's Hospital, Boston, MA 02115, USA
[6]Infectious Diseases Division, Massachusetts Hospital, Boston, MA 02114, USA
[7]Broad Institute of MIT and Harvard, Cambridge, MA 02139, USA
[8]University of Massachusetts Chan Medical School, Worcester, MA 01605, USA
[9]Gastrointestinal Unit, Massachusetts Hospital, Boston, MA 02114, USA
[10]MGH Cancer Center, Massachusetts Hospital, Boston, MA 02114, USA
[11]Monash University, Melbourne, VIC 3800, Australia
[12]Center for the AIDS Programme of Research in South Africa, Durban 4001, South Africa
[13]Department of Microbiology, Harvard Medical School, Boston, MA 02115, USA
[14]Lead contact
*Correspondence: spillai@mgh.harvard.edu
https://doi.org/10.1016/j.celrep.2025.115472

SUMMARY

Memory lymphocytes are durable cells that persist in the absence of antigen, but few human B cell subsets have been characterized in terms of durability. The relative durability of eight non-overlapping human B cell sub-populations covering 100% of all human class-switched B cells was interrogated. Only two long-lived B cell populations persisted in the relative absence of antigen. In addition to canonical germinal center-derived switched-memory B cells with an IgD−CD27+CXCR5+ phenotype, a second, non-canonical, but distinct memory population of IgD−CD27−CXCR5+ DN1 B cells was also durable, exhibited a unique *TP63*-linked transcriptional and anti-apoptotic signature, had low levels of somatic hypermutation, but was more clonally expanded than canonical switched-memory B cells. DN1 B cells likely evolved to preserve immunological breadth and may represent the human counterparts of rodent extrafollicular memory B cells that, unlike canonical memory B cells, can enter germinal centers and facilitate B cell and antibody evolution.

INTRODUCTION

The traditional definition of a memory lymphocyte is of a durable antigen-specific cell that persists and can be activated when re-exposed to its cognate antigen.[1] Canonical, durable memory B cells are traditionally thought to exhibit moderate to high levels of somatic hypermutation (SHM) and to only emerge from a germinal center response.

There are many valid ways to characterize human memory B cells and numerous excellent reviews have described the properties of these cells.[2–4] However, at this time, no categorization scheme for human memory B cells incorporates durability as a criterion. In humans, IgD−CD27+CXCR5+CD21+ CD11c− B cells are conventional switched-memory (SWM) B cells believed to be derived from germinal centers based on the high levels of B cell receptor SHM that they exhibit relative to naive B cells. These cells are relatively durable even in the context of subunit vaccination since durability cannot be convincingly established after live vaccines, infection, or autoimmunity, due to the persistence of antigen. Numerous studies, utilizing varying surface markers, have described many other different class-switched human B cell populations in the context of disease or infection, and many of these cells are referred to as memory B cells, although persistence in the absence or relative absence of antigen has typically not been assessed.

Table 1. Class switched B cell subsets

IgD⁻CD27⁺CXCR5⁺CD11c⁻ (SWM)
IgD⁻CD27⁺CXCR5⁺CD11c⁺ (ABC-like)
IgD⁻CD27⁺CXCR5⁻CD11c⁻ (PB-like)
IgD⁻CD27⁺CXCR5⁻CD11c⁺ (ABC)
IgD⁻CD27⁻CXCR5⁺CD11c⁻ (DN1)
IgD⁻CD27⁻CXCR5⁻CD11c⁺ (DN2)
IgD⁻CD27⁻CXCR5⁻CD11c⁻ (DN3)
IgD⁻CD27⁻CXCR5⁺CD11c⁺ (DN4)

There has been considerable interest in a heterogeneous atypical memory B cell subset often called age-related B cells or ABCs. In rodents, these were described as B220⁺CD19⁺ B cells that do not express CD21, CD23, CD95, or CD43,[5] or as B220⁺CD19⁺CD21⁻ cells that express CD11c.[6] In the same study, Rubtsov et al. examined and defined human CD19⁺CD21⁻CD23⁻CD11c⁺IgD⁻CD27ᴴⁱ human B cells as ABCs.[6] The phenotype of ABCs is linked to the expression of the transcription factors T-bet and ZEB2.[6–8] When ABCs are defined more loosely as Tbet-expressing B cells, they are heterogeneous,[7] and in humans these cells include not only IgD⁻CD27⁺CD11c⁺ cells, but also IgD⁻CD27⁻CD11c⁺ (i.e., double-negative 2 [DN2]) and IgD⁺CD27⁻CD11c⁺ (activated naive) B cells and they are likely closely related to a fairly prominent population of cells that we will refer to below as ABC-like B cells.

When IgD⁻CD27⁺CD11c⁺ ABCs were analyzed in a non-autoimmune and non-infectious context in influenza vaccination-based studies, they were characterized as germinal center-derived B cells since they exhibit robust SHM, but it was also suggested that these cells represent a transient activated B cell population based on their decline in the circulation about 8–10 weeks following vaccination.[9] A second CD11c⁺ class-switched B cell population in the IgD⁻CD27⁻ pool has been studied, especially in the context of systemic lupus erythematosus, and these cells have been referred to as DN2 B cells.[10,11] Sanz and co-workers divided IgD⁻CD27⁻ double-negative (DN) B cells based on their expression of CXCR5 (or CD21, both used interchangeably) and CD11c into two prominent DN B cell subsets, namely, DN1 and DN2 B cells. DN2 B cells are IgD⁻CD27⁻CD11c⁺CXCR5⁻CD21⁻ B cells and similar to CD27⁺ ABCs, display clonal connectivity to plasmablasts. They have been shown to be expanded in many disease states. Based on these data, DN2 B cells represent a CD11c⁺ class-switched B cell subset that can be distinguished from CD27⁺ABCs but likely represent plasmablast precursors that develop outside the germinal center based on their lower frequency of SHM than SWM B cells.[11] Cells with a similar DN1-like phenotype have also previously been reported to have lower SHM levels.[12]

In more recent studies, we described four subsets of antigen-specific DN B cells in the context of SARS-CoV-2 infection, which extended the nomenclature to DN3 and DN4 subsets.[13,14] Sanz and colleagues have also described DN3 B cells in addition in the contexts of COVID-19,[15] and systemic lupus erythematosus.[16] DN3 B cells have a distinct plasmablast-like transcriptional profile and accumulate in non-lymphoid disease end organs far

more readily than DN2 B cells.[14] DN1 B cells in this classification are IgD⁻CD27⁻CD11c⁻CXCR5⁺CD21⁺ B cells. Based on transcriptomic data demonstrating considerable similarity of DN1 B cells to IgD⁻CD27⁺CXCR5⁺ conventional switched memory B cells, these B cells were suggested to potentially represent a type of memory B cell population.[11] In more recent human studies using samples from convalescent COVID-19 patients,[17] a relatively durable CD27⁻ memory B cell population was described (with a CD21⁺CXCR5⁺CD11c⁻ surface phenotype, consistent with DN1 B cells), supporting the notion that there may be an additional *durable* memory B cell population distinct from germinal center-derived canonical IgD⁻CD27⁺CXCR5⁺ memory B cells. However, persisting antigen in any viral infection (or in autoimmunity) prevents firm conclusions regarding durability. The analyses of antigen-specific B cells after influenza vaccination further suggest that the class-switched DN1 CD27⁻ memory B cell population is durable.[18] However, in these previous studies, this subset of B cells was not characterized further in terms of identifying any unique transcriptomic features to convincingly distinguish them from canonical switched memory B cells.

By examining all eight class-switched B cell populations among antigen-specific CD19⁺ IgD⁻ B cells using CD27, CXCR5, and CD11c as markers (Table 1) in a previously uninfected vaccination cohort, as well as in acute and convalescent infection contexts, we were able to conclusively define only two relatively durable class-switched memory B cell populations and six short-lived B cell populations (not including plasmablasts). Among durable memory B cells, one type is the widely studied IgD⁻CD27⁺CXCR5⁺CD11c⁻ canonical class-switched memory B cell population that, as expected, has the hallmarks of being germinal center derived. The second durable class-switched memory B cell population, DN1 B cells, is likely derived outside the germinal center (possibly as part of an extrafollicular response) rather than in the course of a germinal center response. DN1 B cells have lower levels of replacement BCR mutations that span both complementarity determining regions (CDRs) and framework regions (FWRs), they have longer CDRH3s than canonical SWM B cells, but they have clearly previously undergone clonal proliferation since they are more clonally expanded that conventional CD27⁺ memory B cells. These cells can also be clearly distinguished from canonical SWM B cells by a strong *TP63* transcriptome-driven signature. These data define a second bona fide durable human class-switched memory B cell subset, that likely originates outside germinal centers and that may have evolved to contribute to immunological breadth. Six other human class-switched B cell subsets including the more widely studied ABC and DN2 B cell subsets, which can certainly be sustained by autoantigens and persistent infections, are nevertheless all intrinsically non-durable B cell subsets and perhaps should ideally be distinguished from durable memory B cell populations. The term "memory" is widely used in the B cell literature perhaps because issues of durability after antigen decline had not been previously addressed for most populations. In the context of class-switched B cells, we have generally attempted to restrict the use of this term in the remainder of this manuscript to the two durable B cell populations seen.
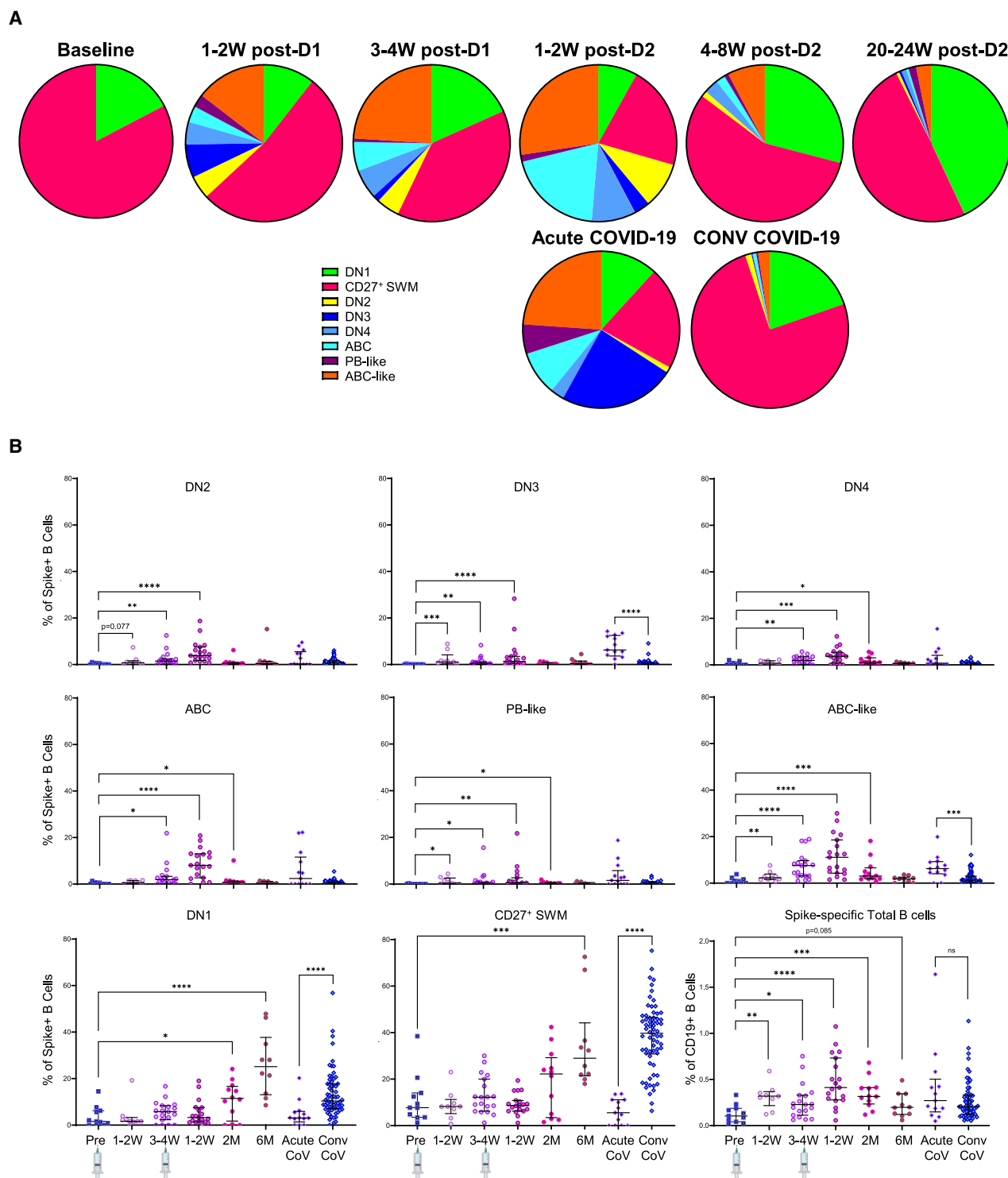
Figure 1. Two durable antigen-specific class-switched B cell populations emerge after vaccination

(A) Pie charts displaying spike-specific B cells profiled from the blood of previously uninfected vaccinees at baseline ($n = 11$), 1–2 weeks post-dose 1 ($n = 9$), time of dose 2 ($n = 19$), 1 week post-dose 2 ($n = 19$), 4–8 weeks post-dose 2 ($n = 12$), and 24 weeks post-dose 2 ($n = 10$), as well as from patients with acute ($n = 13$) or

(legend continued on next page)

RESULTS

Six distinct short-lived activated B cell populations are induced by mRNA vaccination and in acute viral infection

To understand the phenotypes, composition, and cellular kinetics of expansion and contraction vs. persistence over time of antigen-induced human B cells, we interrogated SARS-CoV-2 spike-specific B cells from serially collected blood samples at baseline (pre-vaccination), soon after vaccination (1–2 weeks post-dose 1), at the time of vaccine boost (3–4 weeks post-dose 1), soon after vaccine boost (1–2 weeks post-dose 2), an intermediate duration after vaccine boost (3–4 weeks post-dose 2), and long term after vaccine boost (6 months post-dose 2) from mRNA vaccine recipients (BNT162b2 or mRNA-1273) who had lacked SARS-CoV-2 nucleocapsid responses at baseline (i.e., SARS-CoV-2 naive). These cohorts and time points were also studied alongside acute and convalescent COVID-19 patient samples to establish references for B cell subset composition in infection-induced systemic inflammation vs. non-inflammatory contexts. Hierarchical gating of antigen-specific B cells was employed, and panel design was guided by the literature (Figure S1). Relatively few class-switched B cells were present within the spike-specific B cell gate at the pre-vaccination time point but those present were restricted to just two phenotypes: $IgD^-CD27^+CXCR5^{+CD11c^-}$ (hereafter referred to canonical SWM) and $IgD^-CD27^-CXCR5^+$ $CD11c-$ (double-negative 1, hereafter referred to as DN1) (Figures 1A and 1B). In Figure 1A the denominator is restricted to IgD^-spike^+ B cells (class-switched antigen-specific B cells). In Figure 1B the denominator includes all $spike^+$ B cells.

When examining SARS-CoV-2 spike antigen-specific B cells we observed six distinct short-lived antigen-specific B cell subsets (of which one is extremely minor) that appeared within 1–2 weeks following the first mRNA vaccination dose and generally receded to very low levels by 8 weeks after the second vaccination dose (Figures 1A and 1B). These six short-lived B cell populations were defined by an activated phenotype based on varying combinations of the decreased expression of CXCR5 and CD21 (expression of these two antigens is generally coordinate following B cell activation) and/or the elevated expression of CD11c. For completeness and to ensure we accounted for 100% of class-switched spike-specific B cells, we included the very small population of $CD27^+CXCR5^-CD11c^-$ B cells that have plasmablast-like features (most of these cells are frequently either CD20 low or CD38 high, referred to hereafter as "PB-like"), but this a very minor sub-population. Within the 3–4 weeks following the initiation of vaccination, DN3 B cells and PB-like B cells followed a time course similar to plasmablasts, exhibiting rapid induction within 1–2 weeks followed by quick contraction by weeks 3–4. After the vaccination boost, the most prominent activated B cell subsets that appeared to

most efficiently expand included the $CD27^+CXCR5^-CD11c^+$ (age-associated B cells, hereafter referred to as ABCs), the closely related $CD27^+CXCR5^+CD11c^+$ B cell population that we distinguish by flow but would often also be considered either directly as or as a variant form of $CD27^+$ ABCs (we refer to these cells as "ABC-like"), $CD27^-CXCR5^-CD11c^+$ (double-negative 2, hereafter referred to as DN2), and to a lesser degree, $CD27^-CXCR5^+CD11c^+$ (double-negative 4, hereafter referred to as DN4) subset, suggesting that these types of B cells are preferentially induced upon recall immune responses. The same six short-lived likely activated B cell sub-types were also observed in the setting of acute COVID-19 where the relative expansion of DN3 B cells was the most notable distinguishing feature compared with the mRNA vaccination cohorts, consistent with previous reports (Figures 1A and 1B). The specific surface phenotypes and subset names where appropriate are detailed in Table 1.

Two distinct durable SWM B cell populations are observed following vaccination and in the setting of acute infection and convalescence

By examining spike-specific B cells from SARS-CoV-2-naive mRNA vaccine recipients 20–24 weeks after the second vaccine dose, we observed a stark paucity of all six short-lived B cell populations paired with the relative dominance of DN1 B cells and canonical $CD27^+$ SWM B cells (Figures 1A and 1B). Canonical $CD27^+$ SWM B cells were more prominent, accounting for 20%–80% of antigen-specific B cells at 20–24 weeks, whereas DN1 B cells accounted for 10%–50%. Proportions of spike-specific B cells among the total of $CD19^+$ B cells were higher following each vaccination dose (Figure 1B), concordant with expansion of short-lived activated B cell subsets. In contrast, proportions of spike-specific B cells at the 6-month time point were similar to those of pre-vaccination donors. However, median proportions of DN1 B cells represented approximately 25% of all spike-specific B cells at 6 months compared with under 5% among pre-vaccination donors; those of canonical $CD27^+$ SWM were approximately 30% vs. 8% among pre-vaccination donors. As discussed above, canonical $CD27^+$ SWM and DN1 B cells were the exclusive types of antigen-specific B cells present at the pre-vaccination time point. In contrast, when we examined receptor binding domain (RBD)-specific B cells, there were virtually no antigen-specific class-switched B cells in uninfected, unvaccinated individuals (Figure S2A). These data suggest that all pre-existing class-switched memory B cells against the SARS-CoV-2 S2 domain, which has considerable homology to common cold coronavirus S2 domains, are dominated by canonical $CD27^+$ SWM and DN1 B cells (Figures S2B and S2C).

Both canonical $CD27^+$ SWM and DN1 B cells appeared to reduce proportionally with the early emergence of short-lived activated B cell subsets (1–2 weeks after each vaccination dose) followed by their proportional increase seen at 4–8 weeks after

---

convalescent from COVID-19 ($n = 66$). The median of each B cell subset (as a proportion of all $spike^+IgD^-$ B cells) from each time point are plotted as parts of a whole. DN, double-negative, IgD^-CD27^-; ABC, age-associated B cells; CoV, COVID-19; Conv, convalescent.

(B) Scatterplots displaying the proportion of spike-specific B cell subset and total spike-specific B cells across the same cohorts depicted in (A). Error bars represent medians and interquartile ranges. p values were calculated using the Mann-Whitney test. Asterisks indicate p values with values as follows: $*p = 0.05$ to 0.01, $**p < 0.01$ to >0.001, $***p < 0.001$ to >0.0001, and $****p < 0.0001$.

vaccination boost. Canonical CD27^{+} SWM and DN1 B cells also dominated the antigen-specific B cell composition in the context of convalescence SARS-CoV-2 infection (Conv CoV) and were much less prominent in acute SARS-CoV-2 infection (Acute CoV). Consistent with previous reports, these data supported the existence of two types of memory B cells in humans that follow similar kinetic expansion after exposure to antigen, characterized by the surface phenotype IgD^{−}CXCR5^{+}CD21^{+}CD11c^{−} but distinguished by CD27 expression.[17,18]

DN1 B cells represent a distinct and relatively durable memory B cell population

We next studied a longitudinally collected cohort of convalescent COVID-19 patients with serially collected samples extending as far out as 258 days after symptom onset. Consistent with the findings from our vaccinee cohort, both canonical CD27^{+} SWM and DN1 B cells persisted over time, with the former continuing to proportionally expand and the latter maintaining a plateau in most patients (Figures 2A and 2B). We also examined circulating lymphocytes from a cohort of 24 healthy donors collected prior to the COVID-19 pandemic to understand the distribution of the 6 short-lived and 2 durable memory B cell populations in an antigen-agnostic manner. Consistent with the notion of longevity of canonical CD27^{+} SWM and DN1 B cells, we found these two populations to dominate the circulating IgD^{−} B cell compartment, with the former accounting for a median of 66% (IQR 56%–76%) and the latter 18% (IQR 13%–26%) of all IgD^{−} B cells (Figures 2C and 2D). In contrast, each of the short-lived B cell types contributed median values of under 2% of all IgD^{−} B cells within this cohort, consistent either with their short-lived circulating lifespan or potentially their inability to re-circulate.

DN1 B cells are IgD[−] by definition. To further understand if these cells are truly class-switched memory B cells, we characterized the isotype distribution of the surface BCR and found the majority to have class switched to IgG (mean 74%, SD 9.6%) and a minority to IgA (25%, SD 9.2%) with only a very small proportion to be unswitched with expression of surface IgM (1.3%, SD 0.86%) (Figures 2E and 2F). Both canonical CD27^{+} SWM and DN1 B cells presumably rely on T cell help for their differentiation as supported by their class-switched phenotypes. We observed comparably high levels of surface CD40 expression in both memory subsets, supportive of their ability to interact with cognate T cells (Figure S3). Both memory cell types also express high levels of the chemokine receptor CXCR5 and the selectin CD62L, similar to follicular naive and unswitched memory B cells, suggesting tropism for secondary lymphoid organs (Figure S3).

To better understand dynamic changes in the relative frequencies of these B cell memory types soon after antigen exposure, we examined the phenotype of antigen-specific B cells immediately before and 10 days after a second mRNA vaccination boost. All subjects were 6–7 months past their initial mRNA vaccination series with established B cell memory at the time of vaccine boost. In this relatively short interval, we did not observe significant expansion of antigen-specific B cells as a proportion of all CD19^{+} cells (only 3 of 11 donors showed clear proportional expansion within the entire B cell compartment). In contrast, we found marked shifts in the cellular composition of responding B cells despite the static overall fraction of antigen-specific B cells.

DN1 B cells were consistently reduced and CXCR5^{−}CD11c^{+} short-lived activated B cells (ABCs and DN2 B cells) were consistently expanded across all 11 donors studied (Figure 2G). This observation suggests that DN1 B cells likely respond to antigen re-exposure by activation and differentiation and exhibit the transient dynamic decline expected of memory lymphocytes upon antigen re-exposure.

DN1 B cells exhibit lower rates of SHM and limited positive selection pressure than canonical SWM B cells

We wished to determine if the BCR sequence of DN1 compared with canonical SWM B cells could indicate their potential origins either from within germinal centers or from the extrafollicular response based on the degree of SHM these cells display.

We initially performed bulk IgH CDRH3 region BCR sequencing from FACS-purified naive, DN1, and canonical SWM B cells using the Adaptive platform to quantitate the frequency of SHM. With these analyses, we found DN1 B cells to have a relatively low SHM frequency, closer to the low frequency seen in naive follicular B cells and approximately 3-fold lower than the frequency found in canonical SWM B cells (Figure 3A). In fact, the majority of DN1 B cells showed no mutations whatsoever within their CDRH3 regions (Figure 3B). This was in stark contrast to canonical SWM B cells with nearly all B cells in these groups showing some degree of CDRH3 mutation and typically at a much higher frequency (Figures 3A and 3B). The Adaptive platform provides sequence information on a limited portion of Ig VH genes—primarily the FWR3 and CDR3 regions—and the lengths of CDRH3 regions were seen to be longer in DN1 B cells (and similar to CDRH3 lengths in naive follicular B cells) while CDRH3 length in SWM B cells was markedly reduced (Figure 3C), as has been reported before.[19,20]

To validate these findings and to be able to address issues related to selection of BCRs, we leveraged an orthogonal genomic DNA-based full-length IgH V gene sequencing approach again using FACS-purified B cells from different healthy donors. When quantitating mutational frequency, a measurement of the extent of SHM, naive B cells had the lowest averages of mutational frequencies as expected, DN1 B cells had an intermediate average, and switched memory B cells had the highest average, consistent with our initial findings (Figure 3D). We observed a similar pattern when examining the proportion of non-mutated BCRs with follicular naive B cells having the highest proportion, DN1 B cells showing an intermediate proportion, and canonical SWM having the lowest proportion of non-mutated BCRs (Figure 3E). The longer average CDRH3 length of DN1 B cells compared with canonical SWM was also observed using this approach (Figure 3F). Importantly, we also analyzed replacement to silent mutation ratios for CDRs and FWRs. CDR R/S analyses revealed a degree of replacement mutation frequency among DN1 B cells that was intermediate between follicular naive and canonical SWM B cells (Figure 3G). FWRs in follicular naive B cells exhibited a very low R/S ratio on average, while DN1 and canonical SWM B cells had higher R/S ratios, with canonical memory B cells revealing slightly higher ratios on average relative to DN1 B cells (Figures 3H and 3I).

Examination of repertoire diversity found both DN1 and canonical SWM B cells to exhibit evidence of clonal expansion,
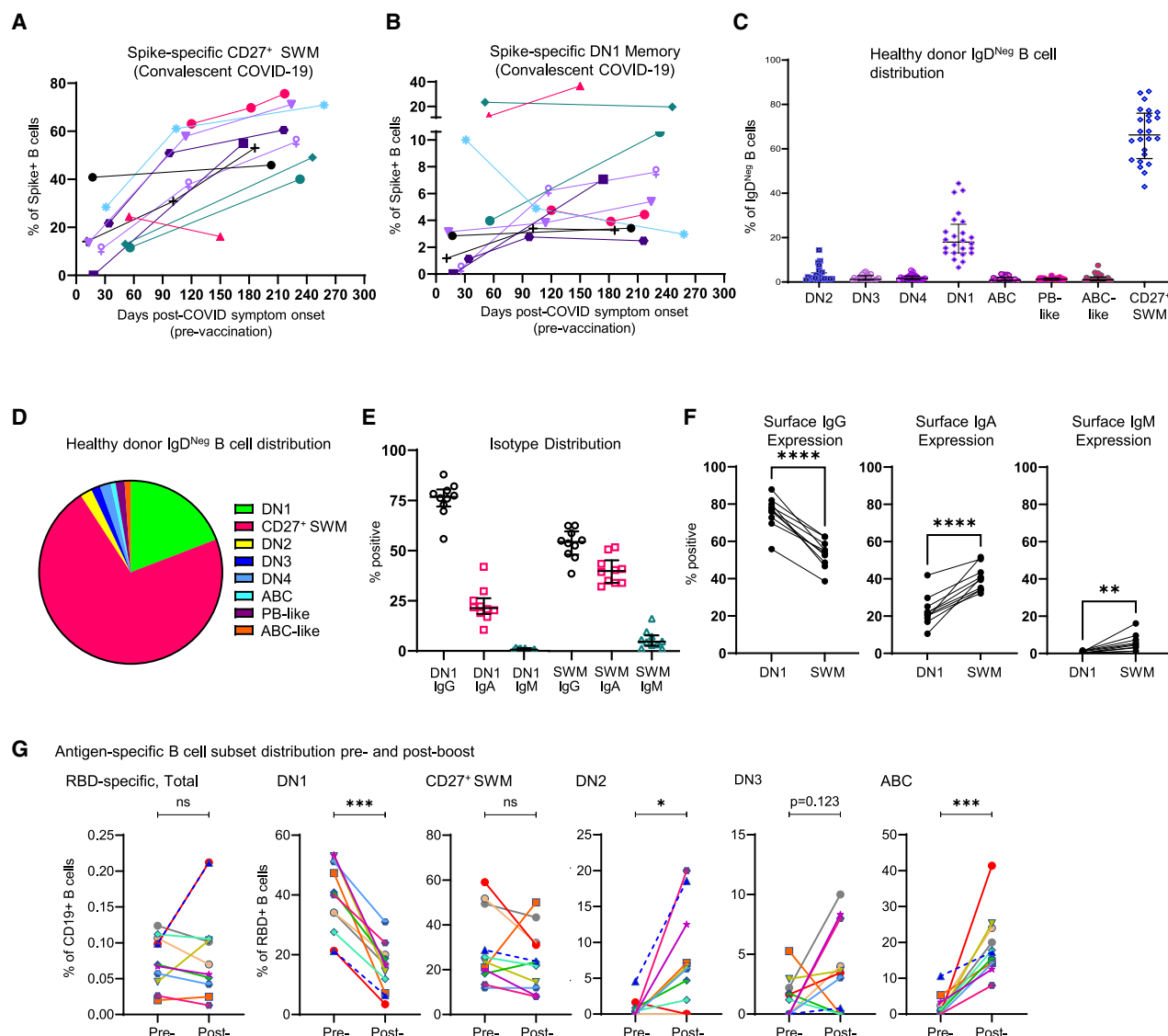
Figure 2. DN1 memory B cells and CD27⁺ SWM B cells accumulate at steady state and during convalescence

(A and B) Dot plots with connecting lines displaying proportions of (A) CD27$^+$ SWM and (B) DN1 B cells among all spike-specific B cells measured longitudinally across 11 patients during convalescence from COVID-19. Each color represents a different patient.

(C) Dot plot displaying proportions of all 8 non-overlapping, non-plasmablast, B cell populations among CD19$^+$IgD$^-$ B cells across 24 pre-pandemic healthy donors. Lo/Lo and Hi/Hi refer to expression levels of CXCR5 and CD11c within the 2 CD27$^+$ B cell subsets.

(D) Pie chart displaying the median values for each B cell subset as parts of a whole representing all non-plasmablast CD19$^+$IgD$^-$ B cells profiled across 24 pre-pandemic healthy donors.

(E) Dot plot displaying the proportions of DN1 B cells expressing IgG, IgA, or IgM at the protein level among healthy donor PBMC samples (*n* = 10).

(F) Dot plots with connecting lines comparing frequencies of IgG, IgA, and IgM surface expression between DN1 and SWM B cells.

(G) Dot plots with connecting lines showing pre- and 10 days post-boost proportions of RBD-specific B cells among all CD19$^+$ B cells (first panel) or of each B cell subset among RBD-specific B cells (subsequent 5 panels) profiled across paired PBMC samples (*n* = 11 from each time point). Each color represents a different donor. Error bars represent medians and interquartile ranges. *p* values were calculated using the Mann-Whitney test. NS, not significant. Asterisks indicate *p* values with values as follows: *p = 0.05 to 0.01, **p < 0.01 to >0.001, ***p < 0.001 to > 0.0001, and ****p < 0.0001.

as supported by reduced BCR diversity relative to follicular naive B cells. Rarefaction curves were generated using a tool initially developed by ecologists to estimate the expected number of species from a sample of a larger diverse group.[21,22] This approach can also help in the estimation of clonal diversity and clonal expansion for antigen receptor sequencing data. We

created rarefaction curves for each sample of naive follicular B cells, DN1 memory B cells, or IgD$^-$CD27$^+$ switched memory B cells for which full-length V gene sequences had been generated. We found that that DN1 memory B cells exhibited the highest amount of clonal expansion compared with switched memory B cells and follicular B cells (Figure 3J). DN1 B cells
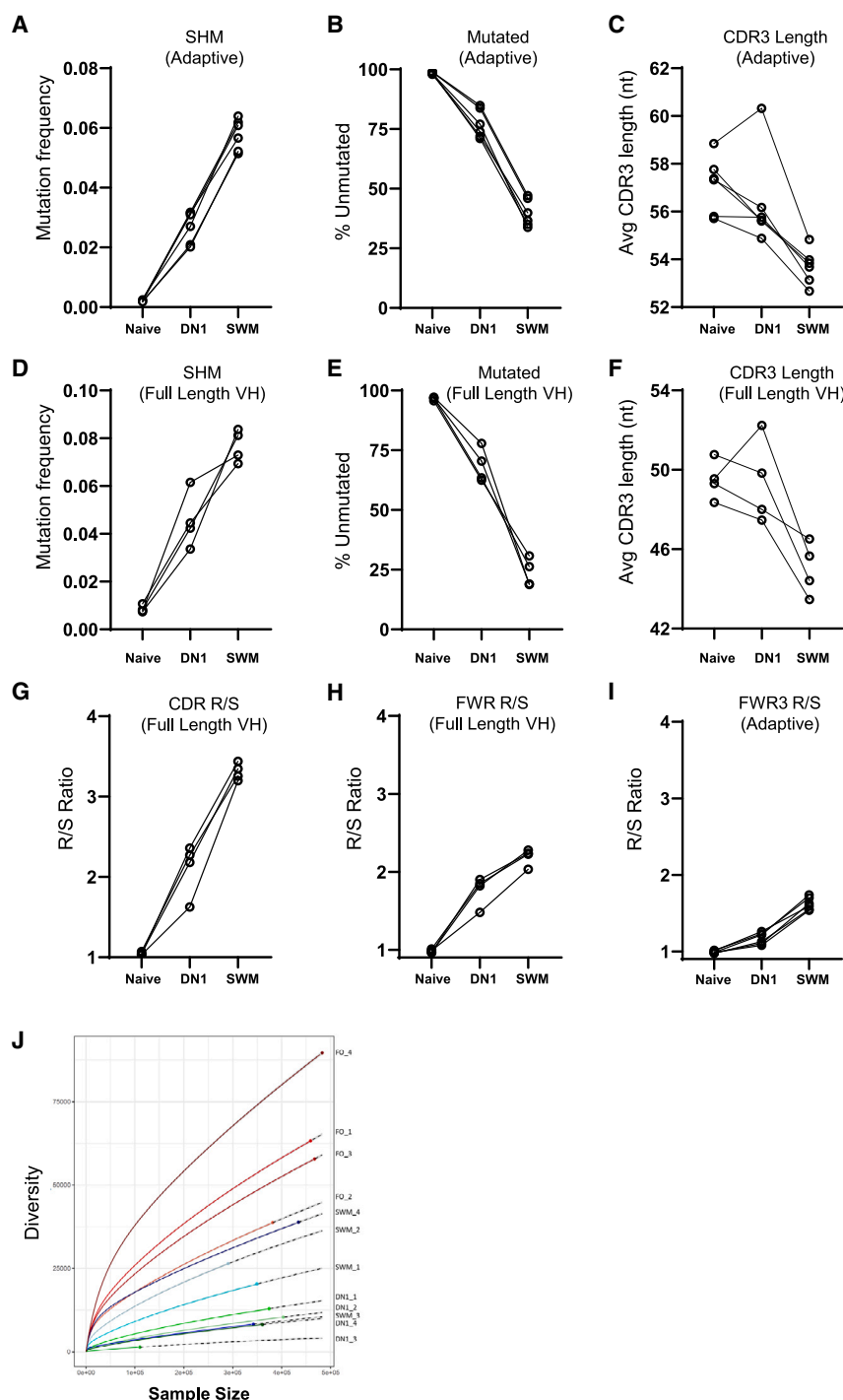
Figure 3. DN1 B cells exhibit lower SHM frequency, less positive selection pressure, and reduced repertoire diversity relative to canonical CD27+ SWM

(A–C) Dot plots with connected lines displaying somatic hypermutation frequency, proportions of BCRs with unmutated germline sequences, and average CDR3 length among flow-purified follicular naive, DN1, and canonical SWM B cells across 6 healthy donor biologic replicates analyzed on the Adaptive platform.

(D–H) Dot plots with connected lines displaying (D) somatic hypermutation frequency, (E) proportions of BCRs with unmutated germline sequences, (F) average CDR3 length, (G) CDR replacement/silent (R/S) mutation ratio, and (H) FWR R/S mutation ratio among flow-purified follicular naive, DN1, and canonical SWM B cells across 4 different healthy donor biologic replicates analyzed by sequencing of the full-length rearranged VH gene.

(I) FWR3 region R/S ratio displayed across the same biologic replicates in (A)–(C) using the Adaptive platform.

(J) Rarefaction curves of follicular, canonical SWM, and DN1 B cells displaying the BCR repertoire diversity (number of unique clones) relative to sequences analyzed for each population. Follicular naive populations are depicted in tones of red, canonical SWM in tones of blue, and DN1 in tones of green. Each rarefaction curve is labeled with the cell population and associated biologic replicate the cells were sorted from. CDR, complementarity determining region; nt, nucleotide; FWR, framework region; FO, follicular. Full-length VH refers to sequencing of the complete VH gene (see STAR Methods).

consistently showed even lower diversity than canonical SWM B cells across the four biologic replicates studied.

DN1 B cells exhibit a distinct TP63-linked transcriptional signature

While there are clear differences in rates of SHM between DN1 B cells and SWM B cells, we wished to ask if DN1 cells can, in a *robust* manner, be distinguished transcriptionally from canonical CD27+ SWM B cells. Transcriptomes for both DN1 and SWM B cell populations have been compared in a limited manner so far.[11] Although we initially conducted CITE-seq and single-cell transcriptomics on pre- and post-vaccination samples, given the broad similarities in the transcriptomes of the DN1 and CD27+IgD− switched memory B cell populations in the studies of Jenks et al.,[11] we recognized the need for deeper, more robust analyses. To determine whether a unique DN1 transcriptomic signature exists, we performed bulk RNA sequencing using sorted follicular naive, DN1, and CD27+ SWM B cells isolated from six healthy control donor PBMCs. PCA clustering revealed strong separation between the three sorted cell populations, including previously undescribed separation between DN1 and canonical SWM B cells along PC2 (Figure 4A). This indicated the presence of a DN1-specific transcriptomic signature in this dataset. Comparing gene expression patterns between the three
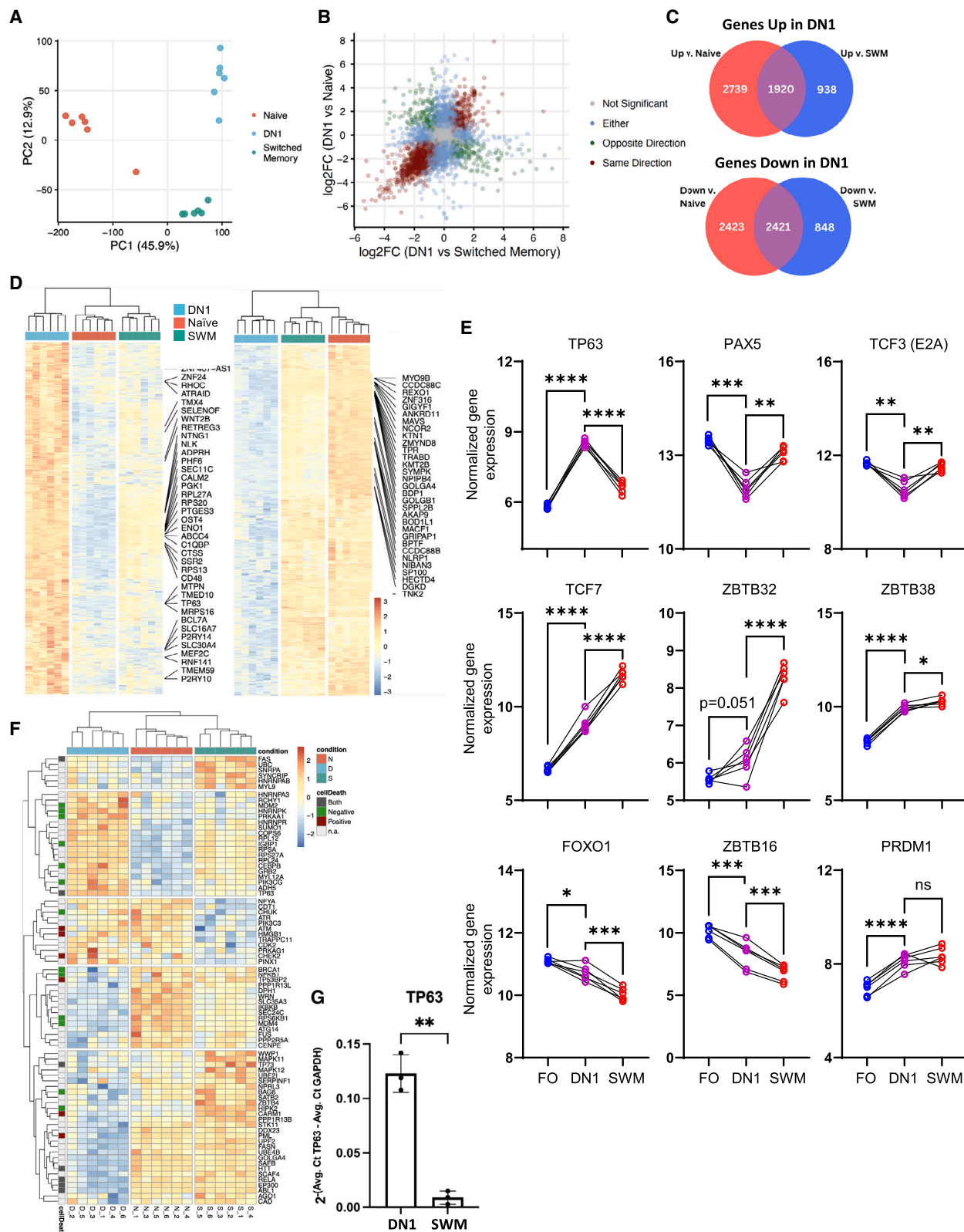
(legend on next page)

sorted B cell populations revealed thousands of differentially expressed genes (DEGs) between DN1 and naive or canonical SWM B cells (Figure 4B). Of these DEGs, 1,920 and 2,421 genes were significantly upregulated and downregulated in DN1, respectively, compared with both naive and SWM B cells (Figure 4C). Heatmaps of the topmost DEGs increased or decreased in DN1 are shown in Figure 4D. To better understand the unique features of DN1 B cells, we used reactome pathway analysis to identify which pathways were significantly enriched in the DEG sets consistently increased or decreased in DN1 (Figures S4A and S4B). Notably, DEGs increased in DN1 were significantly enriched for pathways related to cell metabolism, including "the citric acid cycle and respiratory electron transport" and "cellular response to starvation." DEGs decreased in DN1 were significantly enriched for pathways related to GTPase cycling.

To identify potential drivers of the DN1 transcriptomic signature, we used Regenrich to evaluate gene regulators significantly associated with the identified DEGs.[23] Of the significantly associated gene regulators identified, only *TP63* was strongly increased specifically in DN1, whereas others such as TCF7 and ZBTB16 showed intermediate expression levels among DN1 in between follicular naive and canonical SWM (Figure 4E). *TP63* belongs to a family of transcription factors associated with regulation of cell proliferation and cell death known as the p53 family, which also includes *TP53* and *TP73*. Interestingly, *TP53* and *TP73* were not similarly increased in DN1 B cells (Figure S4C). Because p63 signaling is associated with both positive and negative regulation of cell death, we explored what effect increased *TP63* expression might have on DN1 B cells by evaluating the expression of a *TP63*-driven gene signature across all three B cell populations. This TP63-dependent signature was obtained from the Harmonizome 3.0 database.[24] This identified sub-clusters of genes within the *TP63* signature that demonstrated increased or decreased expression specifically in DN1 (Figure 4F). Of the 19 genes specifically increased in DN1 B cells, 6 were present in the Gene Ontology (GO) annotation "negative regulation of cell death," while none were found in the GO annotation "positive regulation of cell death." These 19 genes increased only in DN1 B cells included *PRKAA1*, the gene that encodes AMPK. Increased *PRKAA1* expression corresponded with a reduction in *MTOR* expression specifically in DN1 B cells (Figure 4F), which relates to previous studies reporting that metabolic reprogramming of B cells, specifically AMPK activation, supports differentiation of unswitched memory B cells to DN B cells.[25] TP63 has been linked to anti-apoptotic signaling

in murine B cells and linked to the induction of BCL-2.[26] The differential expression of *TP63* in DN1 B cells was confirmed using a quantitative RT-PCR approach (Figure 4G). Overall, these data suggest that DN1 B cells possess a unique, *TP63*-driven gene signature that may contribute to their increased durability relative to other B cell subsets as previously described.

DISCUSSION

Our studies reveal that there are two durable class-switched human memory B cell populations that emerge after T-B collaboration, including one that is distinct from the canonical long-studied population that emerges from germinal centers. Not only is the data on durability supported by vaccination studies, it is also consistent with studies on infections and robustly supported by the examination of the accumulation, at steady state, in large numbers of apparently healthy individuals, of discernible class-switched B cells. We would suggest that in humans there are only two class-switched B cell subsets that would fulfill the strict definition of memory by the criteria laid out by Ahmed and Gray.[1] Human IgD⁻CD27⁻CXCR5⁺CD11c⁻DN1 B cells likely emerge outside germinal centers, as suggested by their relatively low frequency of SHM and low R/S ratios compared with canonical SWM B cells. These DN1 B cells are transcriptionally distinguished by the TP63 transcription factor, which can be linked to specific downstream genes, including anti-apoptotic genes, that likely contribute to the distinct biology of DN1 memory B cells. Like canonical SWM B cells, DN1 memory B cells do not express TBX21 and ZEB2, which are, throughout lymphocyte biology, important markers of activated lymphocytes that reciprocally regulate TCF7.[27] It would be appropriate to recognize that the maintenance of intrinsically non-durable DN2 cells and CD27⁺ ABCs in disease contexts likely reflects the ongoing triggering of naive or memory B cells by antigen and the repeated induction of ZEB2 and TBX21. Of course, in autoimmune subjects, the ubiquitous availability of antigen can lead to the persistence of intrinsically non-durable B cell subsets.

We suspect, as has been indicated in the literature, that DN1 B cells like DN2 (and DN3 B cells) emerge from the extrafollicular response.[11] Extrafollicular B cell responses in humans are harder to define because of the difficulty in micro-dissecting lymphoid organs for studies based on the geographical location of cells in secondary lymphoid organs. In our own multicolor immunofluorescence studies, albeit on fixed tissue sections and not

Figure 4. DN1 memory B cells are transcriptionally distinct from canonical SWM B cells and can be defined by a *TP63* linked signature
(A) PCA plot of bulk transcriptomes shows strong separation with respect to sorted B cell sub-populations, including separation between switched memory (green) and DN1 (blue) B cells along PC2 (*N* = 6/group).
(B) Plot showing the number of differentially expressed genes (DEGs) between DN1 and naive (y axis) or SWM B cells (x axis), where each dot represents a gene. Colored dots represent genes with either the same (red) or opposite (green) direction of change in DN1 relative to both naive and SWM.
(C) Venn diagrams showing the number of significantly DEGs that are increased (top) or decreased (bottom) in DN1 B cells compared with naive and/or SWM B cells identified via bulk RNA-seq.
(D) Heatmaps showing the topmost DEGs either increased (left) or decreased (right) in DN1 compared with the other B cell populations.
(E) Plots showing VSD-normalized counts (log-scale) of gene regulators broadly associated with B cell differentiation comparing transcript expression levels across the three B cell populations.
(F) Heatmap showing the expression of a TP63-dependent gene signature across the three B cell populations, where "cellDeath" indicates whether the indicated gene is found in the Gene Ontology (GO) annotation of negative (green) or positive (red) regulation of cell death, or both (gray).
(G) Validation of *TP63* expression in DN1 and SWM B cells using qPCR. Error bars represent means ± SEM.

performed using confocal imaging, IgD⁻CD27⁻BCl-6⁻ B cells in secondary lymphoid organs were primarily localized outside germinal centers, even in control subjects.[13] Nevertheless, the usage here of the term "extrafollicular" should be considered operational rather than geographic. CD27 on human non-plasmablast, class-switched B cells may represent a surface marker for generally establishing the GC origin of canonical SWM B cells and some other activated B cell subsets. Average rates of SHM have therefore been used as a surrogate for GC or non-GC origin of activated and memory B cells. The bias toward an extrafollicular response in lupus may explain why there was a relative impairment of neutralizing activity when lupus patients were vaccinated for COVID-19.[28]

Even with these caveats, we postulate an extrafollicular or possibly more narrowly, an "extra-germinal center" origin for human switched B cell subsets with some caution. Given the higher mutation frequency and replacement to silent mutation ratios of DN1 memory B cells compared with follicular naive B cells, assuming mutations inherently have close to a 1:1 R/S ratio without selection, the results could suggest that DN1 B cells have undergone some degree of SHM and selection, although not to the degree of canonical SWM B cells. This might theoretically have occurred either outside germinal centers or in germinal centers. In the latter scenario, after a few rounds of SHM and selection, DN1 B cells could be postulated to have left the germinal center prematurely. However, a large number of DN1 B cells lack somatic mutations and we believe an origin in a distinct extra-germinal center milieu, likely the extrafollicular T-B boundary, may be permissive for TP63 induction and the development of durable DN1 memory B cells.

The studies of Shlomchik and colleagues on extrafollicular memory B cells in mice have revealed some crucial and important insights regarding the likely unique function of this category of memory B cells.[29] It should be noted that a large fraction of the murine extrafollicular memory B cells identified in those studies are IgM⁺ B cells. These studies reveal that extrafollicular memory B cells can enter germinal centers, while GC-derived memory B cells cannot. The extrafollicular response may thus contribute crucially to durable B cell responses in many unique ways.

It has not been previously considered if there is any distinct, clearly distinguishable, and durable class-switched memory B cell subset with lower levels of SHM and greater immune diversity that may exist potentially and primarily to maintain immunological breadth and to possibly feed into new cycles of germinal center responses with repeated exposure to antigens. We speculate that DN1 memory B cells have evolved to retain broad memory to inciting pathogens so that the same or variant pathogens can in subsequent infections utilize these cells to more robustly enter new germinal centers and to initiate affinity matured antibody responses. Such notions can best be tested in appropriate rodent models and indeed murine DN1 like B cells may be a subset of the cells studied by Callahan et al.[29]

Overall, these data indicate that DN1 B cells are a durable class-switched human memory B cell population that is likely derived through T-dependent B cell activation in the course of an extrafollicular response in secondary lymphoid organs. Although these cells exhibit limited SHM they undergo relatively large clonal expansions. DN1 B cells can be distinguished from canonical CD27⁺ SWM B cells since the latter exhibit high SHM, shorter CDRH3s on average, less B cell clonal expansion, and have the hallmarks of being derived from germinal centers. In addition, we establish here a TP63-linked transcriptome and associated anti-apoptotic signature that defines and distinguishes DN1 memory B cells from canonical SWM B cells. These data suggest an important evolutionary role for this memory B cell subset in maintaining broad immunologic antigen recognition breadth in contrast to the narrower affinity-matured recognition mediated by canonical SWM B cells.

The p63 protein family has been best studied in epithelial cells and most lymphocyte subsets do not express the TP63 gene. Intriguingly, in many different categories of epithelial cells, differential promoter usage in the TP63 gene can give rise to two major categories of p63 protein; one arising from longer transcripts that encodes TAp63, which possesses an N-terminal transactivation domain. This protein has an anti-apoptotic function. Usage of a distal promoter facilitates the generation of ΔNp63, a protein that mediates epithelial stemness in many different epithelial tissues.[30] It remains to be seen, potentially by the study of genetically engineered mice, whether TP63 in the B lineage sustains a stem-like self-renewing memory B cell population.

Limitations of the study

Finding differences in gene expression of TP63 and potential target genes between DN1 B cells and CD27⁺IgD⁻ switched memory B cells does not establish a functional role for TP63 in the DN1 B cell population. Further studies at the chromatin level in human B cells may help further validate potential transcriptional targets of TP63, but the B lineage-specific knockout of tp63 in mice will be required to convincingly establish the function of this gene in B lineage cells. No methods exist to conclusively determine the site of origin in humans (from the germinal center or not) of any category of human memory B cells.

Our studies were restricted to the peripheral blood. It is possible that some switched B cell subsets are sequestered in tissues and our studies were not designed to assess that possibility. Our studies were also not powered to detect differences in memory B cell subsets following vaccination or infection based on age, sex, race, or ethnicity. Larger studies would be needed to determine the influence of these demographic variables on the induction of memory B cell subsets.

RESOURCE AVAILABILITY

Lead contact

Further information and requests for resources and reagents should be directed to and will be fulfilled by the lead contact, Shiv Pillai (pillai@helix.mgh.harvard.edu).

Materials availability

The SARS-CoV-2 RBD and spike proteins were made freely available through Dr. Aaron Schmidt during the pandemic but are now available from many commercial sources.

Data and code availability

- De-identified RNA sequencing data have been deposited in the GEO database at GEO: accession number GEO: GSE278378 and are publicly available as of the date of publication.
- This paper does not report original code.

- Any additional information required to reanalyze the data reported in this paper is available from the lead contact upon request.

AUTHOR CONTRIBUTIONS

Study design/conceptualization, S.P., C.A.P., and J.M.; execution, C.A.P., H.L., J.M., T.V.G., N.I., J.L., and Z.M.; reagent generation, J.F., C.J.-D., B.M.H., A.S., A.B.B., D.L., and A.G.S.; computational analyses, design, and integration, A.P., A.H., N.C., and W.T.; patient recruitment and sample processing, V.N., R.C., J.A.I., A.M.-R., A.M., K.N., M.B.B., J.E.L., D.R.W., Z.M.-H., O.O., C.B., F.S., M.A.G., R.T.-M., C.K., Z.Z., and A.N.; writing and integration, S.P., C.A.P., and J.M.

DECLARATION OF INTERESTS

S.P. is on the Scientific Advisory Boards of Paratus Inc., BeBiopharma Inc., Octagon Therapeutics, and AbPro Inc., all activities unrelated to the studies described here.

STAR★METHODS

Detailed methods are provided in the online version of this paper and include the following:

- KEY RESOURCES TABLE
- EXPERIMENTAL MODEL AND STUDY PARTICIPANT DETAILS
  - Cell lines
  - Study participants
- METHOD DETAILS
  - Human samples
  - Protein expression and purification
  - Flow cytometry and tetramer generation
  - Bulk RNA sequencing
  - RNA sequencing analysis
  - Bulk BCR sequencing
  - TP63 quantitative PCR
- QUANTIFICATION AND STATISTICAL ANALYSIS

SUPPLEMENTAL INFORMATION

Supplemental information can be found online at https://doi.org/10.1016/j.celrep.2025.115472.

REFERENCES

1. Ahmed, R., and Gray, D. (1996). Immunological memory and protective immunity: understanding their relation. Science 272, 54–60. https://doi.org/10.1126/science.272.5258.54.

2. Weisel, F., and Shlomchik, M. (2017). Memory B Cells of Mice and Humans. Annu. Rev. Immunol. 35, 255–284. https://doi.org/10.1146/annurev-immunol-041015-055531.

3. Cancro, M.P., and Tomayko, M.M. (2021). Memory B cells and plasma cells: The differentiative continuum of humoral immunity. Immunol. Rev. 303, 72–82. https://doi.org/10.1111/imr.13016.

4. Inoue, T., and Kurosaki, T. (2024). Memory B cells. Nat. Rev. Immunol. 24, 5–17. https://doi.org/10.1038/s41577-023-00897-3.

5. Hao, Y., O'Neill, P., Naradikian, M.S., Scholz, J.L., and Cancro, M.P. (2011). A B-cell subset uniquely responsive to innate stimuli accumulates in aged mice. Blood 118, 1294–1304. https://doi.org/10.1182/blood-2011-01-330530.

6. Rubtsov, A.V., Rubtsova, K., Fischer, A., Meehan, R.T., Gillis, J.Z., Kappler, J.W., and Marrack, P. (2011). Toll-like receptor 7 (TLR7)-driven accumulation of a novel CD11c(+) B-cell population is important for the development of autoimmunity. Blood 118, 1305–1315. https://doi.org/10.1182/blood-2011-01-331462.

7. Cancro, M.P. (2020). Age-Associated B Cells. Annu. Rev. Immunol. 38, 315–340. https://doi.org/10.1146/annurev-immunol-092419-031130.

8. Dai, D., Gu, S., Han, X., Ding, H., Jiang, Y., Zhang, X., Yao, C., Hong, S., Zhang, J., Shen, Y., et al. (2024). The transcription factor ZEB2 drives the formation of age-associated B cells. Science 383, 413–421. https://doi.org/10.1126/science.adf8531.

9. Lau, D., Lan, L.Y.L., Andrews, S.F., Henry, C., Rojas, K.T., Neu, K.E., Huang, M., Huang, Y., DeKosky, B., Palm, A.K.E., et al. (2017). Low CD21 expression defines a population of recent germinal center graduates primed for plasma cell differentiation. Sci. Immunol. 2, eaai8153. https://doi.org/10.1126/sciimmunol.aai8153.

10. Kaminski, D.A., Wei, C., Qian, Y., Rosenberg, A.F., and Sanz, I. (2012). Advances in human B cell phenotypic profiling. Front. Immunol. 3, 302. https://doi.org/10.3389/fimmu.2012.00302.

11. Jenks, S.A., Cashman, K.S., Zumaquero, E., Marigorta, U.M., Patel, A.V., Wang, X., Tomar, D., Woodruff, M.C., Simon, Z., Bugrovsky, R., et al. (2018). Distinct Effector B Cells Induced by Unregulated Toll-like Receptor 7 Contribute to Pathogenic Responses in Systemic Lupus Erythematosus. Immunity 49, 725–739.e6. https://doi.org/10.1016/j.immuni.2018.08.015.

12. Fecteau, J.F., Côté, G., and Néron, S. (2006). A new memory CD27-IgG+ B cell population in peripheral blood expressing VH genes with low frequency of somatic mutation. J. Immunol. 177, 3728–3736. https://doi.org/10.4049/jimmunol.177.6.3728.

13. Kaneko, N., Kuo, H.H., Boucau, J., Farmer, J.R., Allard-Chamard, H., Mahajan, V.S., Piechocka-Trocha, A., Lefteri, K., Osborn, M., Bals, J., et al. (2020). Loss of Bcl-6-Expressing T Follicular Helper Cells and Germinal Centers in COVID-19. Cell 183, 143–157. https://doi.org/10.1016/j.cell.2020.08.025.

14. Allard-Chamard, H., Kaneko, N., Bertocchi, A., Sun, N., Boucau, J., Kuo, H.H., Farmer, J.R., Perugino, C., Mahajan, V.S., Murphy, S.J.H., et al. (2023). Extrafollicular IgD(-)CD27(-)CXCR5(-)CD11c(-) DN3 B cells infiltrate inflamed tissues in autoimmune fibrosis and in severe COVID-19. Cell Rep. 42, 112630. https://doi.org/10.1016/j.celrep.2023.112630.

15. Woodruff, M.C., Ramonell, R.P., Nguyen, D.C., Cashman, K.S., Saini, A.S., Haddad, N.S., Ley, A.M., Kyu, S., Howell, J.C., Ozturk, T., et al. (2020). Extrafollicular B cell responses correlate with neutralizing antibodies and morbidity in COVID-19. Nat. Immunol. 21, 1506–1516. https://doi.org/10.1038/s41590-020-00814-z.

16. Jenks, S.A., Wei, C., Bugrovsky, R., Hill, A., Wang, X., Rossi, F.M., Cashman, K., Woodruff, M.C., Aspey, L.D., Lim, S.S., et al. (2021). B cell subset composition segments clinically and serologically distinct groups in chronic cutaneous lupus erythematosus. Ann. Rheum. Dis. 80, 1190–1200. https://doi.org/10.1136/annrheumdis-2021-220349.

17. Zurbuchen, Y., Michler, J., Taeschler, P., Adamo, S., Cervia, C., Raeber, M.E., Acar, I.E., Nilsson, J., Warnatz, K., Soyka, M.B., et al. (2023). Human memory B cells show plasticity and adopt multiple fates upon recall response to SARS-CoV-2. Nat. Immunol. 24, 955–965. https://doi.org/10.1136/annrheumdis-2021-220349.

18. Andrews, S.F., Chambers, M.J., Schramm, C.A., Plyler, J., Raab, J.E., Kanekiyo, M., Gillespie, R.A., Ransier, A., Darko, S., Hu, J., et al. (2019). Activation Dynamics and Immunoglobulin Evolution of Pre-existing and Newly Generated Human Memory B cell Responses to Influenza Hemagglutinin. Immunity 51, 398–410.e5. https://doi.org/10.1016/j.immuni.2019.06.024.

19. Rosner, K., Winter, D.B., Tarone, R.E., Skovgaard, G.L., Bohr, V.A., and Gearhart, P.J. (2001). Third complementarity-determining region of mutated VH immunoglobulin genes contains shorter V, D, J, P, and N components than non-mutated genes. Immunology *103*, 179–187. https://doi.org/10.1046/j.1365-2567.2001.01220.x.

20. DeKosky, B.J., Lungu, O.I., Park, D., Johnson, E.L., Charab, W., Chrysostomou, C., Kuroda, D., Ellington, A.D., Ippolito, G.C., Gray, J.J., and Georgiou, G. (2016). Large-scale sequence and structural comparisons of human naive and antigen-experienced antibody repertoires. Proc. Natl. Acad. Sci. USA *113*, E2636–E2645. https://doi.org/10.1073/pnas.1525510113.

21. Sanders, H.L. (1968). Marine Benthic Diversity: A Comparative Study. Am. Nat. *102*, 243–282. http://www.jstor.org/stable/2459027.

22. Hurlbert, S.H. (1971). The Nonconcept of Species Diversity: A Critique and Alternative Parameters. Ecology *52*, 577–586. https://doi.org/10.2307/1934145.

23. Tao, W., Radstake, T.R.D.J., and Pandit, A. (2022). RegEnrich gene regulator enrichment analysis reveals a key role of the ETS transcription factor family in interferon signaling. Commun. Biol. *5*, 31. https://doi.org/10.1038/s42003-021-02991-5.

24. Rouillard, A.D., Gundersen, G.W., Fernandez, N.F., Wang, Z., Monteiro, C.D., McDermott, M.G., and Ma'ayan, A. (2016). The harmonizome: a collection of processed d. Database *2016*, baw100. https://doi.org/10.1093/database/baw100.

25. Torigoe, M., Iwata, S., Nakayamada, S., Sakata, K., Zhang, M., Hajime, M., Miyazaki, Y., Narisawa, M., Ishii, K., Shibata, H., and Tanaka, Y. (2017). Metabolic Reprogramming Commits Differentiation of Human CD27(+) IgD(+) B Cells to Plasmablasts or CD27(-)IgD(-) Cells. J. Immunol. *199*, 425–434. https://doi.org/10.4049/jimmunol.1601908.

26. Lantner, F., Starlets, D., Gore, Y., Flaishon, L., Yamit-Hezi, A., Dikstein, R., Leng, L., Bucala, R., Machluf, Y., Oren, M., and Shachar, I. (2007). CD74 induces TAp63 expression leading to B-cell survival. Blood *110*, 4303–4311. https://doi.org/10.1182/blood-2007-04-087486.

27. Dominguez, C.X., Amezquita, R.A., Guan, T., Marshall, H.D., Joshi, N.S., Kleinstein, S.H., and Kaech, S.M. (2015). The transcription factors ZEB2 and T-bet cooperate to program cytotoxic T cell terminal differentiation in response to LCMV viral infection. J. Exp. Med. *212*, 2041–2056. https://doi.org/10.1084/jem.20150186.

28. Faliti, C.E., Van, T.T.P., Anam, F.A., Cheedarla, N., Williams, M.E., Mishra, A.K., Usman, S.Y., Woodruff, M.C., Kraker, G., Runnstrom, M.C., et al. (2025). Disease-associated B cells and immune endotypes shape adaptive immune responses to SARS-CoV-2 mRNA vaccination in human SLE. Nat. Immunol. *26*, 131–145. https://doi.org/10.1038/s41590-024-02010-9.

29. Callahan, D., Smita, S., Joachim, S., Hoehn, K., Kleinstein, S., Weisel, F., Chikina, M., and Shlomchik, M. (2024). Memory B cell subsets have divergent developmental origins that are coupled to distinct imprinted epigenetic states. Nat. Immunol. *25*, 562–575. https://doi.org/10.1038/s41590-023-01721-9.

30. Senoo, M., Pinto, F., Crum, C.P., and McKeon, F. (2007). p63 is essential for the proliferative potential of stem cells in stratified epithelia. Cell *129*, 523–536. https://doi.org/10.1016/j.cell.2007.02.045.

31. Dobin, A., Davis, C.A., Schlesinger, F., Drenkow, J., Zaleski, C., Jha, S., Batut, P., Chaisson, M., and Gingeras, T.R. (2013). STAR: ultrafast universal RNA-seq aligner. Bioinformatics *29*, 15–21. https://doi.org/10.1093/bioinformatics/bts635.

32. Putri, G.H., Anders, S., Pyl, P.T., Pimanda, J.E., and Zanini, F. (2022). Analysing high-throughput sequencing data in Python with HTSeq 2.0. Bioinformatics *38*, 2943–2945. https://doi.org/10.1093/bioinformatics/btac166.

33. Yu, G., and He, Q.Y. (2016). ReactomePA: an R/Bioconductor package for reactome pathway analysis and visualization. Mol. Biosyst. *12*, 477–479. https://doi.org/10.1039/C5MB00663E.

34. Rosenfeld, A.M., Meng, W., Horne, K.I., Chen, E.C., Bagnara, D., Stervbo, U., and Luning Prak, E.T.; AIRR Community (2022). Bulk gDNA Sequencing of Antibody Heavy-Chain Gene Rearrangements for Detection and Analysis of B-Cell Clone Distribution: A Method by the AIRR Community. Methods Mol. Biol. *2453*, 317–343. https://doi.org/10.1007/978-1-0716-2115-8_18.

35. Bolotin, D.A., Poslavsky, S., Mitrophanov, I., Shugay, M., Mamedov, I.Z., Putintseva, E.V., and Chudakov, D.M. (2015). MiXCR: software for comprehensive adaptive immunity profiling. Nat. Methods *12*, 380–381. https://doi.org/10.1038/nmeth.3364.

36. Shugay, M., Bagaev, D.V., Turchaninova, M.A., Bolotin, D.A., Britanova, O.V., Putintseva, E.V., Pogorelyy, M.V., Nazarov, V.I., Zvyagin, I.V., Kirgizova, V.I., et al. (2015). VDJtools: Unifying Post-analysis of T Cell Receptor Repertoires. PLoS Comput. Biol. *11*, e1004503. https://doi.org/10.1371/journal.pcbi.1004503.

37. Gupta, N.T., Vander Heiden, J.A., Uduman, M., Gadala-Maria, D., Yaari, G., and Kleinstein, S.H. (2015). Change-O: a toolkit for analyzing large-scale B cell immunoglobulin repertoire sequencing data. Bioinformatics *31*, 3356–3358. https://doi.org/10.1093/bioinformatics/btv359.

STAR★METHODS

KEY RESOURCES TABLE

REAGENT or RESOURCES	SOURCE	IDENTIFIER
Antibodies		
Anti-CD3	Miltenyi Biotec	Clone BW264/56
Anti-CD19	BioLegend	Clone SJ25C1
Anti-CD27	BD Biosciences	Clone L128
Anti-IgD	BioLegend	Clone IA6-2
Anti-CD38	BioLegend	Clone HIT2
Anti-CD21	BD Biosciences	Clone B-ly4
Anti-CD11c	BD Biosciences	Clone B-ly6
Anti-CXCR5	BD Biosciences	Clone RF8B2
Anti-CD20	BD Biosciences	Clone 2H7
Anti-IgG	BD Biosciences	Clone G18-145
Anti-IgA	Miltenyi Biotec	Clone IS11-8E10
Anti-IgM	BD Biosciences	Clone G20-127
Anti-CD40	BioLegend	Clone 5C3
Anti-CD62L	BioLegend	Clone DREG-56
Anti-CXCR4	BioLegend	Clone 12G5
Anti-IGF-1R	BioLegend	Clone 1H7/CD221
Anti-CD11c-TotalSeq-C	BioLegend	Clone S-HCL-3
Anti-CD20-TotalSeq-C	BioLegend	Clone 2H7
Anti-CXCR5-TotalSeq-C	BioLegend	Clone J252D4
Anti-CD27-TotalSeq-C	BioLegend	Clone O323
Anti-CD21-TotalSeq-C	BioLegend	Clone Bu32
Anti-IgD-TotalSeq-C	BioLegend	Clone IA6-2
Anti-CD38-TotalSeq-C	BioLegend	Clone HIT2
Anti-CD73-TotalSeq-C	BioLegend	Clone AD2
Anti-CD85j-TotalSeq-C	BioLegend	Clone GHI/75
Anti-PE Streptavidin-TotalSeq-C	BioLegend	CAT# 504155
Anti-CD45RB-TotalSeq-C	BioLegend	Clone MEM-55
Anti-CD10-TotalSeq-C	BioLegend	Clone HI10a
Anti-human Hashtag 1 Antibody	BioLegend	CAT#394661
Anti-human Hashtag 2 Antibody	BioLegend	CAT#394663
Anti-human Hashtag 3 Antibody	BioLegend	CAT#394665
Anti-human Hashtag 4 Antibody	BioLegend	CAT#394667
Anti-human Hashtag 5 Antibody	BioLegend	CAT#394669
Anti-human Hashtag 6 Antibody	BioLegend	CAT#394671
Anti-human Hashtag 7 Antibody	BioLegend	CAT#394673
Anti-human Hashtag 8 Antibody	BioLegend	CAT#394675
Anti-human Hashtag 9 Antibody	BioLegend	CAT#394677
Chemicals and recombinant proteins		
FcR Blocking Reagent	Miltenyi Biotec	CAT#130-059-901
Rainbow Calibration Particles	ThermoFisher	CAT#A34305
DRAQ7 Dead cell exclusion dye	BioLegend	CAT# 424001
Streptavidin-APC conjugate	ThermoFisher	CAT#S32362
Streptavidin-PE conjugate	BioLegend	CAT#405204

(Continued on next page)

Continued

REAGENT or RESOURCES	SOURCE	IDENTIFIER
Strep-Tactin APC	IBA-Lifesciences	CAT#6-5010-001
Strep-Tactin PE	IBA-Lifesciences	CAT#6-5010-001
Deposited data		
RNA sequencing data	GEO Database	Accession # GEO: GSE278378
Recombinant DNA		
pVRC-SARS-CoV-2-RBD WA1/2020 and Omicron variant	Schmidt Lab	N/A
pCAGGS-SARS-CoV-2 spike WA-1 2020 and Omicron variant	McClellan/Balazs/Schmidt Labs	N/A
Software and algorithms		
FlowJo	FlowJo	www.flowjo.com
FACSDIVA	BD Biosciences	www.bdbiosciences.com/en-us/instruments/research-instruments/research-software/flow-cytometry-acquisition/facsdiva-software
Prism 8	GraphPad Software	www.graphpad.com/scientific-software/prism/
CellRanger (v6.0.1)	10X Genomics	https://support.10xgenomics.com/single-cell-vdj/software/
R (v4.1.1)	R	www.r-project.org/
Seurat (v4.0.6)	Seurat	satijalab.org/seurat/
IgBlast (online server)	National Library of Medicine	www.ncbi.nlm.nih.gov/igblast/

EXPERIMENTAL MODEL AND STUDY PARTICIPANT DETAILS

Cell lines
Expi293F cells were tested for Mycoplasma contamination by qPCR.

Study participants
All participants provided informed consent prior to sample collection as approved by the Institutional Review Boards at the Massachusetts General Hospital and the University of Massachusetts Medical School. Eleven participants from a pre-vaccination timepoint were included with a median age of 51, 27% male, 73% female, 55% Caucasian, 18% African American, and 27% Hispanic. Nine participants donated blood from a timepoint of 1–2 weeks after vaccine dose 1 with a median age of 56, 56% male, 44% female, 89% Caucasian, 11% African American, and 0% Hispanic. Nineteen participants donated blood from a timepoint of 3–4 weeks after vaccine dose 1 with a median age of 60, 47% male, 53% female, 89% Caucasian, 11% African American, and 0% Hispanic. Nineteen participants donated blood from a timepoint of 1–2 weeks after vaccine dose 2 with a median age of 61, 42% male, 58% female, 89% Caucasian, 11% African American, and 0% Hispanic. Twelve participants donated blood from a timepoint of 4–8 weeks following vaccine dose 2 with a median age of 66, 58% male, 42% female, 100% Caucasian, 0% African American, and 0% Hispanic. Ten participants donated blood from a time point of 24 weeks following vaccine dose 2 with a median age of 44, 30% male, 70% female, 80% Caucasian, 0% African American, and 20% Hispanic. For all vaccination cohorts, lack of exposure to SARS-CoV-2 was determined by measuring serologic responses to SARS-CoV-2 Nucleocapsid antigens. Thirteen patients with acute COVID-19 were recruited with a median age of 62, 54% male, 46% female, 54% Caucasian, 8% African American, and 54% Hispanic. Acute COVID-19 was defined by active symptoms of pneumonia and ongoing hospitalization for SARS-CoV-2 infection as confirmed by RT-PCR. Sixty-six patients with convalescent COVID-19 were recruited with a median age of 39, 36% male, 64% female, 72% Caucasian, 2% African American, and 24% Hispanic. Convalescent COVID-19 was defined as a clinically asymptomatic state on the date of blood draw after recovering from a prior symptomatic SARS-CoV-2 infection or serologic evidence of prior infection. Twenty-one healthy donors were recruited prior to March 2020 and had a median age of 66 and consisted of 52% males and 48% females. Healthy donor status was defined by the lack of any ongoing or historic infectious, autoimmune, or malignant condition, as determined by review of the medical record.

METHOD DETAILS

Human samples
Peripheral blood samples were drawn from patients with COVID-19 at Massachusetts General Hospital and vaccinees at MGH and the University of Massachusetts Medical Center. PBMCs were stored in liquid nitrogen for subsequent batch experiments. For

vaccination cohorts, antibodies to the spike protein receptor binding domain and nucleocapsid were measured by the Roche Elecsys Anti-SARS-CoV-2 S and Anti-N assay (Roche Diagnostics, Indianapolis, IN), per manufacturer's instructions. Uninfected and unvaccinated subjects were defined by having no detectable anti-spike or anti-nucleocapsid antibodies. For patients with acute COVID-19, the median number of days from symptom onset to blood draw was 28 and the interquartile range was 14–29 days. For convalescent COVID-19 donors, 58 of 66 convalescent donors had symptomatic infection with well-defined dates of symptom onset. For these donors, the median number of days from symptom onset to blood draw was 217 and the interquartile range was 174–248 days. Eight of the 66 convalescent COVID-19 patients had been previously asymptomatic but were identified by the presence of anti-SARS-CoV-2 spike or anti-nucleocapsid responses at the time of blood draw and prior to vaccination, and duration of infection could not be determined. Demographic and clinical data related to vaccinated and COVID-19 cohorts are described under STAR Methods and detailed in Tables S1 and S2. Healthy donor samples used in Figures 2C and 2D were all historic PBMCs collected prior to March of 2020.

Sample pairing: Among vaccinee cohorts, 47% of week 3–4 post dose 1 samples were paired with subjects from week 1–2 post dose 1, 89% of week 1–2 post dose 2 samples were paired with subjects from week 3–4 post dose 1, and 92% of week 4–8 post dose 2 samples were paired with subjects from week 1–2 post dose 2. Five of 6 subjects from the week 1 post dose 3 time point were paired with subjects from the week 24 post dose 2 time point. Additional details related to sample pairing across cohorts are available in Table S1.

Protein expression and purification

SARS-2 RBD (GenBank: MN975262.1) was cloned into pVRC vector containing an HRV 3C-cleavable C-terminal His8X and Avi-tags and sequence confirmed by Genwiz. SARS-CoV-2 full-length spike protein contained a C-terminal foldon trimerization domain and His8X and Avi tags (Wrapp et al., 2020). The constructs were transiently transfected into mammalian Expi293F suspension cells for recombinant expression. Five to seven days post-transfection, supernatants were harvested by centrifugation and purified by immobilized metal affinity chromatography (IMAC) using Cobalt-TALON resin (Takara) followed by size exclusion chromatography on Superdex 200 Increase 10/300 GL (GE Healthcare) in PBS. Purity was assessed by SDS-PAGE analysis. Purified RBD proteins were site-specifically biotinylated using the BirA biotin-protein ligase kit (Avidity) following manufacturer's instructions.

Flow cytometry and tetramer generation

Cryopreserved PBMCs in aliquots of 5–10 million cells were thawed quickly at 37°C and DMSO rapidly diluted with 1% BSA in PBS. Cells were incubated at 21°C for 15 min prior to transfer to FACS tubes for centrifugation. All centrifugation steps were carried out at 1,250 RPM at 4°C. Prior to antibody staining, Fc receptors were blocked using human FcR blocking reagent (Miltenyi) at a concentration of 1:20 at 4°C for 10 min. For antigen-specific experiments, we generated two distinct antigen-specific tetramer probes, each labeled with a different fluorophore, combined with a broader flow cytometry panel to characterize all class-switched B cell subsets. For all spike-specific studies, tetramers were generated using Strep-Tagged proteins and fluorescent Strep-Tactin probes. Strep-Tactin APC (IBA-Lifesciences, CAT#6-5010-001) and Strep-Tactin PE (IBA-Lifesciences, CAT#6-5010-001) were used for dual labeling of antigen-specific B cells. An optimal staining ratio of Strep-Tagged antigen to Strep-Tactin probe of 25 nM antigen to 0.5 μL Strep-Tactin was empirically determined and used consistently for all experiments.

For RBD-specific studies, tetramers were generated using site-specific biotinylated proteins and fluorescent streptavidin probes. Wild-type RBD was separately complexed with Streptavidin-APC (ThermoFisher, CAT#S32362) and Streptavidin-PE (BioLegend, CAT#405204). Complexes were formed using an antigen to streptavidin molar ratio of 4:1 for all RBD experiments.

Tetramers were generated at the time of each experiment. Each antigen plus probe dilution was mixed as described above and incubated at 4°C for 45-min protected from light. Cells were surface stained first at 37°C, protected from light, using optimized concentrations of fluorochrome-conjugated primary antibodies for 20 min. Cells were then washed, centrifuged, and resuspended in a separate 4°C antibody master mix for an additional 30-min stain at 4°C. Antigen complexes were added to the 4°C master mix. Finally, cells were washed, centrifuged, and re-suspended in DRAQ7 dead cell exclusion dye (BioLegend) at a concentration of 1:1000. DRAQ7 is a membrane-impermeable dye with an emission maxima of 678/697 nm once intercalated with dsDNA. We designed our flow panel with CD3 on APC/R700 and CD19 on APC/Cy7 such that any cells with dual-emission across these two channels was considered non-viable and excluded (as displayed in Figure S1). As shown in the comprehensive gating strategy (Figure S1), CD38 high plasmablasts were not quantitated during flow cytometric analyses because our primary focus was to identify memory B cell subsets and the staining approach employed was not designed for optimal capture of plasmablasts with low or no surface BCR. Antibodies used with manufacturer, clone, conjugate and staining information are as follows: anti-human CD3 (Miltenyi Biotec, Clone BW264/56, APC-R700, 1:200, 4°C); anti-human CD19 (BioLegend, Clone SJ25C1, APC-Cy7, 1:25, 4°C); anti-human CD27 (BD Biosciences, Clone L128, BUV395, 1:40, 4°C); anti-human CD27 (BioLegend, Clone M-T271, PE-Dazzle, 1:100, 4°C); anti-human IgD (BioLegend, Clone IA6-2, BV785, 1:100, 37°C); anti-human-CD38 (BioLegend, Clone HIT2, BV421, 1:100, 4°C); anti-human-CD21 (BD Biosciences, Clone B-ly4, BV480, 1:100, 37°C); anti-human CD11c (BD Biosciences, Clone B-ly6, BV605, 1:100, 4°C); anti-human CXCR5 (BD Biosciences, Clone RF8B2, A488, 1:100, 37°C), anti-human CD20 (BD Biosciences, Clone 2H7, BUV805, 1:100, 37°C); anti-human IgG (BD Biosciences, Clone G18-145, BB700, 1:100, 4°C); anti-human IgA (Miltenyi Biotec, Clone IS11-8E10, APC, 1:100, 4°C); anti-human IgM (BD Biosciences; Clone G20-127, BUV395, 1:25, 4°C). All flow cytometry was performed on a

BD Symphony cytometer (BD Biosciences, San Jose, CA) and rainbow tracking beads (8 peaks calibration beads, Fisher) were used to ensure consistent cytometer signal output between flow cytometry experiments.

Bulk RNA sequencing

Naive (CD19^{+} CD20^{+} IgD + CD27^{−} CXCR5+ CD11c-), DN1 (CD19^{+} CD20^{+} IgD- CD27^{−} CXCR5+ CD11c-), and SWM (CD19^{+} CD20^{+} IgD- CD27^{+} CXCR5+ CD11c-) B cells were FACS purified from cryopreserved PBMC's using a FACS Aria Fusion cell sorter. Total RNA was isolated from sorted B cell populations using the RNAeasy Plus Micro kit (Qiagen) according to the manufacturer's instructions. RNA quality was assessed via Agilent 4200 Tapestation and RNA concentration was determined using a Qubit Flex (Fisher Scientific). Total RNA (4 ng/sample) was processed using the SMARTer Stranded Total RNA-seq Kit v3-Pico Input Mammalian (Takara). Final libraries were quantified with a Tapestation (Agilent) prior to dilution and pooling for sequencing on a NextSeq 2000 (Illumina) using 2x100 bp paired-end chemistry.

RNA sequencing analysis

The reads in each sample were mapped to human reference genome GrCh38 using STAR software (version 2.7.9a).[31] On average, we obtained ~11.3 million uniquely mapped reads per sample. Raw read count matrix (the number of reads for each gene in each sample) was obtained using HTSeq python package (version 2.0.1).[32] The genes with less than 5 reads on average in all samples were removed, resulting 26,777 genes remaining for further analysis. The differential expression analyses between different cell populations were performed using likelihood ratio test (LRT) in DESeq2 R package (version 1.38.1). Genes with FDR-adjusted p-value <0.05 were considered differentially expressed genes (DEG). Raw read count data was normalized using variance stabilizing transformation (VST) to obtain VST-transformed data (VSD), which was used for generating principal component analysis plots and visualization of individual gene expression. Pathway enrichment analysis was performed using ReactomePA R package (version 1.41.1).[33] The regulator enrichment analysis was performed using RegEnrich R package (version 1.8.0).[23]

Bulk BCR sequencing

Naive (CD19^{+} CD20^{+} IgD + CD27^{−} CXCR5+ CD11c-), DN1 (CD19^{+} CD20^{+} IgD- CD27^{−} CXCR5+ CD11c-), and SWM (CD19^{+} CD20^{+} IgD- CD27^{+} CXCR5+ CD11c-) B cells were FACS purified from freshly isolated PBMC's using a FACS Aria Fusion cell sorter. Cells were directly sorted into DNA LoBind tubes containing DNA RNA Sheild (Zymo). Genomic DNA was isolated from each lysate using Quick-DNA/RNA Microprep Plus Kits (Zymo), per manufacturer's protocol. Full-length heavy chain sequences were amplified using equimolar VH and JH primer cocktails and Multiplex PCR Kits (Qiagen), as previously described.[34] IGH PCR products were enriched using AMPure bead purification following the manufacturer's protocol (Beckman Coulter). Illumina barcodes and indices were added with a 2nd round of PCR using Multiplex PCR Kits (Qiagen).[34] Barcoded PCR products were run through 2% agarose gel and gel purified using a QIAquick Gel Extraction Kit (Qiagen). Each PCR product was quantified on Qubit using a dsDNA high-sensitivity kit and equimolar libraries were prepared. Libraries were sequenced using a 600 cycle MiSeq Kit v3 and an Illumina MiSeq sequencer.

For Antibody gene repertoire analyses, IGHV gene BCR sequences were aligned with MiXCR,[35] and subsequently analyzed with VDJtools,[36] and Shazam, a part of the Immcantation framework for Adaptive Immune Receptor Repertoire (AIRR) analyses.[37]

TP63 quantitative PCR

From the same cell lysates described under the bulk BCR sequencing section, RNA was purified using Quick-DNA/RNA Microprep Plus Kits (Zymo), per manufacturer's protocol. Reverse transcription was performed using Applied Biosystems' High-Capacity cDNA Reverse Transcriptino kit (catalog #4374966). Real-time PCR was next performed using Applied Biosystems' TaqMan Gene Expression Assay for TP63 (Hs00978340_m1) and TaqMan Fast Advanced Master Mix (catalog #4444557). Thermocycling was carried out using a BioRad T100 Thermal Cycler for 40 cycles and Applied Biosystems' ViiA 7 Real-Time PCR System was used to analyze the expression of TP63.

QUANTIFICATION AND STATISTICAL ANALYSIS

FCS files were analyzed, and B cell subsets were quantified using FlowJo software (version 10). GraphPad Prism version 8 was used for all statistical analyses and plotting of data points. For comparison of paired samples, the Wilcoxon matched-pairs signed rank test, or the Friedman test was used to calculate p-values, depending on the distribution of the data. For comparing unpaired datasets, the Mann Whitney U test was used. A p-value of <0.05 was considered significant.